

## **Supporting Information for**

## **Completion of Lunar Magma Ocean Solidification at 4.43 Ga**

Nicolas Dauphas<sup>1\*</sup>, Zhe J. Zhang<sup>1</sup>, Xi Chen<sup>1</sup>, Mélanie Barboni<sup>2</sup>, Dawid Szymanowski<sup>3,4</sup>, Blair Schoene<sup>4</sup>, Ingo Leya<sup>5</sup>, Kevin D. McKeegan<sup>6</sup>

<sup>1</sup>Origins Laboratory, Department of the Geophysical Sciences and Enrico Fermi Institute, The University of Chicago, Chicago IL 60637, USA.

<sup>2</sup>School of Earth and Space Exploration, Arizona State University, Tempe, AZ 85281, USA.

<sup>3</sup>Institute of Geochemistry and Petrology, ETH Zurich, 8092 Zurich, Switzerland.

<sup>4</sup>Department of Geosciences, Princeton University, Princeton, NJ 08544, USA.

<sup>5</sup>Space Sciences and Planetology, University of Bern, Bern 3012, Switzerland.

<sup>6</sup>Department of Earth, Planetary, and Space Sciences, University of California, Los Angeles, CA 90095, USA.

Corresponding author: Nicolas Dauphas

Email: [dauphas@uchicago.edu](mailto:dauphas@uchicago.edu)

### **This PDF file includes:**

Supporting text  
Figures S1 to S7  
Tables S1  
SI References

### **Other supporting materials for this manuscript include the following:**

Datasets S1

## Supporting Information Text

Unless otherwise noted, error bars are 95% confidence intervals.

### 1. Samples

The analyzed zircon grains analyzed were extracted from Apollo samples by gently crushing the samples, separating dense minerals using heavy liquid methylene iodide, and handpicking zircon fragments from the high density ( $>3.3 \text{ g/cm}^3$ ) fraction under UV light (1). To maximize the zircon yield, heavy residues were then put on double-sided tape, put in a Tescan SEM coupled with EDS at UCLA and each grain was tested for zirconium. The zircons were mounted in epoxy and characterized using cathodoluminescence to avoid grains with obvious complex growth patterns. The zircons were then dated using U-Pb by Secondary Ion Mass Spectrometry (SIMS) to make sure that these were ancient lunar zircons suitable for Lu-Hf study. As discussed below, the ages of these zircons were re-measured using U-Pb Isotope Dilution-Thermal Ionization Mass Spectrometry (ID-TIMS), which is a more precise technique, so the SIMS U-Pb ages are only used for selecting old zircons. In total, 36 zircon grains were studied using the same protocol. Chen *et al.* (2) previously reported Hf isotopic data for 5 zircon grains (14163 z9, 14163 z89, 14163 z26, 14321 z3, 72275 z1), and Barboni *et al.* (3) reported Hf isotopic data for additional 6 zircon grains (14311,58 z7, 14311,58 z21, 14311,58 z37, 14163,65 z3, 14163,65 z7, 15405,75 z1). We report here data for 25 new zircon grains, and we use the data from the 11 reported zircon grains from Chen *et al.* (2) and Barboni *et al.* (3), as these zircons were analyzed using the exact same protocol, and dating KREEP crystallization was not the scope of those studies. Chen *et al.* (2) used 5 small zircon grains to test the methodology, while Barboni *et al.* (3) focused on the 4.338 Ga peak in the U-Pb age distribution, so they only report Hf data for zircon grains with U-Pb ages between 4334 and 4338 Ma. Zircons in igneous clasts are rare, and they are usually found as individual grains in breccia matrices or as detrital grains in soil samples (4). Little direct information is therefore lost by not knowing the petrographic context of their occurrences. The zircons were extracted from the following samples (as indicated in the zircon labels)(5):

- 26 zircon grains from Apollo 14 "14311". Sample 14311 is an impact melt breccia (3204 g) from a site covered by the Fra Mauro Formation, which is thought to contain ~15 to 60% ejecta from the Imbrium impact basin (6, 7). The matrix (75-95% of the total volume) is melted and recrystallized, reacting with the clasts that comprise various mineral (plagioclase, pyroxene, Fe-Ti oxides) and lithic (igneous rocks and older impact breccias) fragments (5). The exposure age of this breccia is ~550-660 Myr (8, 9). Zircons from this breccia have been extensively characterized for their U-Pb ages, REE patterns, and Ti-thermometry (3, 4, 10, 11). They are crystals and fragments predating breccia formation (10). These zircons yield concordant U-Pb ages spanning ~3.95 to ~4.35 Ga. The ages are unevenly distributed, defining peaks at 4.337, 4.240, 4.110, 4.030, and 3.960 Ga that could reflect crystallization from impact melt sheets associated with large impacts. The REE composition of the oldest zircon population is like that of granite and gabbro-norite clasts. Barboni *et al.* (3) report Hf isotopic data for 3 of the 24 zircon grains from this sample (z9, z21, z37). We report data for 21 new zircon grains from this sample (z57, z8, z7, z18, z38, z43, z69, z71, z40, z15, z12, z47, z59, z61, z64, z6, z58, z60, z34, z24, and z27).
- 7 zircon grains from the Apollo 14 "14163" bulk soil sample (7776 g). It contains a large percentage of glass; most of it (46-61%) in the form of agglutinates. Smaller soil size fractions contain abundant granitic glass (12, 13). Zircons from that soil have U-Pb ages that are mostly concordant and span ~3.95 to 4.35 Ga (3, 14). Data for 3 out of those 7 zircons were presented in Chen *et al.* (2) (z9, z89, z26). Data for 2 additional zircon grains were presented in Barboni *et al.* (3) (14163\_65 z3, 14163\_65 z7). We report data for 2 new zircon grains from this sample (14163\_65 z4 and 14163\_949 z3).
- 1 zircon grain from Apollo 15 "15405". Sample 15405 is a breccia (513.1 g) containing mineral fragments as well as lithic clasts of KREEP-rich basalt, granite, and quartz monzodiorite. The matrix has a similar composition to KREEP-rich basalts. U-Pb dating of zircons indicates relatively recent Pb-loss presumably associated with formation of the breccia (4, 15), but concordant ages of up to 4.3-4.4 Ga are found (3, 4, 14, 15). Data for this zircon grain was presented in Barboni *et al.* (3) (14163\_75 z1). No new data are reported here.
- 1 zircon grain from Apollo 14 "14321". Sample 14321 is a clast-rich crystalline matrix breccia (8998 g) sampled very near the Cone crater. The matrix is mostly crystalline. The clasts are diverse in

- composition, including basalt, troctolite, anorthosite, dunite, and granite. Granite clast 14321,1027 (16) contains a zircon dated at 3.965 Ga (4). Anorthosite clast 14321.16 contains a zircon dated at 4.02-4.05 Ga (17). More zircons without petrographic context have been dated using U-Pb and the ages span the range 3.9-4.4 Ga (3, 14, 17-19). Data for zircon grain z3 was reported in Chen *et al.* (2). No new data are reported here.
- 1 zircon grain from Apollo 17 72275A. Sample 72275 is a feldspathic polymict breccia (3640 g) with ~60% matrix and ~40% clasts. It may represent ejecta from the Serenitatis basin. Most zircons from this breccia have U-Pb ages of 4.24-4.37 Ga (3, 14, 20), with one zircon holding a record precise concordant age of  $4.417 \pm 6$  Ma (20), which represents a minimum age for lunar formation. Various clast types have been documented, including a coarse-grained granitic clast (72275,520; Fig. 1 of Meyer *et al.* 1996) (4). Data for 1 zircon grain was reported in Chen *et al.* (2), which was also compiled by Barboni *et al.* (3) (z1). No new data are reported here.

## 2. Sample processing and U-Pb-Lu-Hf isotopic analyses

Sample processing and isotopic analyses were explained in Chen *et al.* (2). That paper also contains an in-depth discussion of cosmogenic effects and their correction, as well as error propagation during data reduction and model age calculation. The reader is referred to that publication for details and only a summary is provided below.

U-Pb analyses were done at Princeton University following methods described in detail in Barboni *et al.* (3). The zircons were first thermally annealed (48 h at 900 °C), then subjected to a partial dissolution procedure (3, 21, 22) producing two leachates (L1 and L2) and one residue (R) solution, with L1+L2+R corresponding to total digestion. Each zircon was first treated with 100  $\mu$ L 29 M HF+15  $\mu$ L 3 M HNO<sub>3</sub> for 6 h in a Parr bomb held at 180 °C. The leachate, along with solutions from several rinses of the residual zircon with different acids (particularly HCl, aimed at dissolving fluorides) were collected as solution named L1. Each zircon was then treated a second time under the same conditions (100  $\mu$ L 29 M HF+15  $\mu$ L 3 M HNO<sub>3</sub> for 6 h at 180 °C). This solution is named L2. The residual zircon was finally dissolved in a Parr bomb using 100  $\mu$ L 29 M HF+15  $\mu$ L 3 M HNO<sub>3</sub> for 48 h at 210 °C. This solution is named R. Each solution was spiked and equilibrated with the EARTHTIME (<sup>202</sup>Pb-)<sup>205</sup>Pb-<sup>233</sup>U-<sup>235</sup>U spike. Uranium and lead were separated from the rest of the matrix by column chromatography using AG1-X8 resin. The matrix eluted from the U-Pb column was dried down and subsequently redissolved in 0.5 M HNO<sub>3</sub> + 0.015 M HF + 1 ppb In. About 30% of the volume was used for analysis of Lu/Hf elemental ratio and trace elements using standard-sample bracketing in an iCAP single collector ICP-MS at Princeton University. The trace element concentrations are given in Datasets S1. The remaining 70% of the solution was dried down and shipped to the Origins Lab of the University of Chicago for Hf purification and isotopic analysis. The Lu/Hf elemental ratios were measured again using standard-sample bracketing by Multi collector ICPMS at the University of Chicago prior to Hf purification. The results agree with iCAP measurements and are compiled in Datasets S1. The Lu/Hf ratios used to correct for <sup>176</sup>Lu-decay in the zircons are those measured at Princeton.

A 2-column procedure was used to purify Hf from all other elements. The first column was filled with 2 mL of TODGA resin (2, 23, 24). The sample was loaded, and the matrix eluted in 20 mL of 12 M HNO<sub>3</sub>. Titanium was then eluted with 10 mL of 12 M HNO<sub>3</sub>-1% H<sub>2</sub>O<sub>2</sub>. Iron was then eluted with 10 mL of 3 M HNO<sub>3</sub>. Hafnium and zirconium were then eluted together in 20 mL of 3 M HNO<sub>3</sub>-0.3 M HF. The Zr+Hf elution cut was then dried down and loaded in 0.5 mL of 2.5 M HCl on a second column filled with 0.35 mL Ln-Spec (2, 25, 26). The matrix was eluted with 12 mL of 6 M HCl-1% H<sub>2</sub>O<sub>2</sub>. Zirconium was eluted with 22 mL of 6 M HCl-0.06 M HF. Pure Hf was finally eluted in 7 mL of 6 M HCl-0.2 M HF.

Each U-Pb elution was dried down and loaded on a single outgassed zone-refined Re filament with some Si-gel emitter (27) for isotopic analysis using an Isotopx Phoenix Thermal Ionization Mass Spectrometer (TIMS) equipped with ATONA amplifiers at Princeton University (3, 28). Analytical methods were identical to those reported in Barboni *et al.* (3). The calculated U-Pb ages are compiled in Table S1 and Datasets S1.

Hafnium isotopic composition was measured at the Origins Lab of the University of Chicago using a Neptune Multi Collector Inductively Coupled Plasma Mass Spectrometer (MC-ICP-MS) (2) upgraded to Neptune Plus specifications with a Pfeiffer OnTool Booster turbo pump. Purified Hf was introduced into the mass spectrometer in 0.3 M HNO<sub>3</sub>-0.07 M HF using an Aridus II desolvating nebulizer at an uptake rate of 100  $\mu$ L/min. Jet sample and X-skimmer cones were used, and the measurements were made in low resolution.

Isotopes  $^{172}\text{Yb}$ ,  $^{174}\text{Hf}$ ,  $^{175}\text{Lu}$ ,  $^{176}\text{Hf}$ ,  $^{177}\text{Hf}$ ,  $^{178}\text{Hf}$ ,  $^{179}\text{Hf}$ ,  $^{180}\text{Hf}$ , and  $^{184}\text{Hf}$  were measured on Faraday cups connected either to  $10^{12} \Omega$  amplifiers for  $^{172}\text{Yb}$  and  $^{174}\text{Hf}$ , or  $10^{11} \Omega$  amplifiers for all other isotopes. The solutions were diluted to 1-10 ppb Hf for analysis. Under optimal conditions, the sensitivity of the instrument was 0.2 V of  $^{177}\text{Hf}^+/\text{ppb Hf}$ . Sample measurements were bracketed by analyses of JMC-Hf 475 standard solution diluted to a concentration that matched that of the sample. Bracketing analyses were repeated until the sample solution was nearly empty. *On peak zero* ion intensities were measured on a clean 0.3 M  $\text{HNO}_3$ -0.07 M HF solution. The amounts of Hf analyzed for each zircon and the corresponding spherical-equivalent grain diameter are compiled in Table S1. These are minimum estimates as the zircon grains were plucked out of epoxy mounts and the original grains were larger, having been polished for SIMS analysis. The minimum equivalent diameter is  $d = \left( \frac{6m_{\text{Hf}}}{\pi\rho_{\text{zircon}}[\text{Hf}]_{\text{zircon}}} \right)^{1/3}$ , where  $m_{\text{Hf}}$  is the mass of Hf calculated for original zircons (combination of 30% for trace elements, and 70% for Hf isotope determinations),  $\rho_{\text{zircon}}$  is the density of zircon ( $\sim 4.6 \text{ g/cm}^3$ ), and  $[\text{Hf}]_{\text{zircon}}$  is the concentration of Hf in zircon ( $\sim 1 \text{ wt}\%$ ). Numerically, this takes the form,  $d [\mu\text{m}] = 34.63(m_{\text{Hf}} [\text{ng}])^{1/3}$ .

Isobaric interferences of  $^{176}\text{Yb}$ ,  $^{176}\text{Lu}$ , and  $^{180}\text{W}$  were monitored at masses  $^{172}\text{Yb}$ ,  $^{175}\text{Lu}$ , and  $^{184}\text{W}$  and were corrected for. They were always negligible. No attempt was made at correcting any contribution of  $^{180}\text{Ta}$  because it is a very low abundance isotope (0.012 %). Hafnium isotopic ratios  $^i\text{Hf}/^{177}\text{Hf}$  were corrected for instrumental mass fractionation by internal normalization to a fixed  $^{179}\text{Hf}/^{177}\text{Hf}$  ratio of 0.7325. Hafnium isotopic composition is expressed relative to the value of the JMC-Hf 475, which is used to bracket the sample measurements in a sequence Standard-Sample-Standard,

$$\varepsilon^i\text{Hf}_{\text{sample},j} = \left[ \frac{(^i\text{Hf}/^{177}\text{Hf})_{\text{sample},j}^*}{0.5(^i\text{Hf}/^{177}\text{Hf})_{\text{standard},j-1}^* + 0.5(^i\text{Hf}/^{177}\text{Hf})_{\text{standard},j+1}^*} - 1 \right] \times 10^4, \quad (\text{S1})$$

where  $(^i\text{Hf}/^{177}\text{Hf})^*$  denotes the internally normalized ratio. When the sample solution was analyzed multiple times during sample-standard bracketing, the average of all bracketed  $\varepsilon^i\text{Hf}_{\text{sample},j}$  values was used. The standard error of this mean was calculated based on the standard deviation of the standards bracketed by themselves. The errors thus calculated were compared by Chen *et al.* (2) to theoretical predictions for the minimum attainable precision imposed by counting statistics and Johnson noise, and the reproducibility achieved was in all cases very close to the theoretical limit. The measured results and propagated errors are compiled in Datasets S1.

### 3. Zircon U-Pb geochronology

The U-Pb ages of 36 zircons were measured in this study in L1, L2, and R. The results are plotted in Fig. S1. The first leachates (L1) were often discordant and not included in this discussion. The second leachates (L2) and residues are mostly near-concordant (within  $\sim 0.3\%$  for their  $^{207}\text{Pb}/^{235}\text{U}$  and  $^{206}\text{Pb}/^{238}\text{U}$  ages). Some L2 leachates show reversely discordant ( $^{206}\text{Pb}/^{238}\text{U}$  ages  $> ^{207}\text{Pb}/^{235}\text{U}$  ages), caused by elemental fractionation of U from Pb. As discussed in Barboni *et al.* (3), this is likely an artifact from the partial dissolution process, rather than a problem associated with open system behavior of the zircons. The obtained  $^{206}\text{Pb}$ - $^{207}\text{Pb}$  ages of L2 are mostly consistent with the residues of the same zircon grain, varying from 3939 to 4338 Ma (Fig. S1).

### 4. Initial $\varepsilon^{176}\text{Hf}$ values

The initial  $^{176}\text{Hf}/^{177}\text{Hf}$  ratio of a zircon after correction of cosmogenic effects and Lu-decay is calculated relative to the chondritic uniform reservoir (CHUR) in  $\varepsilon$ -notation ( $\varepsilon^{176}\text{Hf}_{\text{zrc}-t,c/\text{CHUR}-t}$ ) as (2),

$$\varepsilon^{176}\text{Hf}_{\text{zrc}-t,c/\text{CHUR}-t} = \left[ \frac{\left( \frac{^{176}\text{Hf}}{^{177}\text{Hf}} \right)_{\text{zrc}-p} \left( 1 - \frac{\alpha_i \varepsilon^i\text{Hf}}{10^4} \right) - \left( \frac{^{176}\text{Lu}}{^{177}\text{Hf}} \right)_{\text{zrc}-p} (e^{\lambda_{176}t} - 1)}{\left( \frac{^{176}\text{Hf}}{^{177}\text{Hf}} \right)_{\text{CHUR}-ss} + \left( \frac{^{176}\text{Lu}}{^{177}\text{Hf}} \right)_{\text{CHUR}-p} (e^{\lambda_{176}t_{ss}} - e^{\lambda_{176}t})} - 1 \right] \times 10^4, \quad (\text{S2})$$

where  $\alpha_i$  is the coefficient that relates cosmogenic effects of  $\varepsilon^{176}\text{Hf}$  and  $\varepsilon^i\text{Hf}$  with  $i = 178$  and  $180$  ( $\alpha_{178} = +2.35 \pm 0.25$  or  $\alpha_{180} = -1.54 \pm 0.11$ ) (2),  $\lambda_{176} = 1.867 \pm 0.008 \times 10^{-11} \text{ yr}^{-1}$  is the decay constant of  $^{176}\text{Lu}$  calibrated based on isochron analyses of terrestrial rocks with known ages (29) (a more recent estimate based on laboratory decay counting provides a consistent value of  $1.864 \pm 0.003 \times 10^{-11} \text{ yr}^{-1}$  (30)),  $t$  is the independently known age from U-Pb dating,  $t_{ss} = 4567.30 \pm 0.16 \text{ Myr}$  is the age of the solar system (31),  $c$  stands for corrected for cosmogenic effects,  $p$  stands for present,  $\left( \frac{^{176}\text{Hf}}{^{177}\text{Hf}} \right)_{\text{zrc}-p}$  and

$(^{176}\text{Lu}/^{177}\text{Hf})_{\text{zrc}-p}$  are ratios measured in the zircon at present,  $(^{176}\text{Hf}/^{177}\text{Hf})_{\text{CHUR}-ss} = 0.279781 \pm 0.000018$  is the CHUR isotopic composition at the formation of the solar system (26), and  $(^{176}\text{Lu}/^{177}\text{Hf})_{\text{CHUR}-p} = 0.0338 \pm 0.0001$  is the CHUR Lu/Hf ratio at present (26). The  $(^{176}\text{Lu}/^{177}\text{Hf})_{\text{CHUR}-p}$  estimate of Izuka *et al.* (26) of  $0.0338 \pm 0.0001$  is close to the estimate of Bouvier *et al.* (32) of  $0.0336 \pm 0.0001$ . For calculating errors, we follow Chen *et al.* (2) and split the uncertainties originating from zircon analyses from those arising from CHUR by writing,

$$\begin{aligned} \varepsilon^{176}\text{Hf}_{\text{zrc}-t,c/\text{CHUR}-t} &= \varepsilon^{176}\text{Hf}_{\text{zrc}-t,c/\text{CHUR}-t} - \varepsilon^{176}\text{Hf}_{\text{CHUR}-t/\text{CHUR}-t} = \\ &= \left[ \frac{\left( \frac{^{176}\text{Hf}}{^{177}\text{Hf}} \right)_{\text{zrc}-p} \left( 1 - \frac{\alpha_i \varepsilon^i \text{Hf}}{10^4} \right) - \left( \frac{^{176}\text{Lu}}{^{177}\text{Hf}} \right)_{\text{zrc}-p} (e^{\lambda_{176}t} - 1)}{\left( \frac{^{176}\text{Hf}}{^{177}\text{Hf}} \right)_{\text{CHUR}-ss} + \left( \frac{^{176}\text{Lu}}{^{177}\text{Hf}} \right)_{\text{CHUR}-p} (e^{\tilde{\lambda}_{176}t_{ss}} - e^{\tilde{\lambda}_{176}t})} - 1 \right] \times 10^4 - \\ &= \left[ \frac{\left( \frac{^{176}\text{Hf}}{^{177}\text{Hf}} \right)_{\text{CHUR}-ss} + \left( \frac{^{176}\text{Lu}}{^{177}\text{Hf}} \right)_{\text{CHUR}-p} (e^{\lambda_{176}t_{ss}} - e^{\lambda_{176}t})}{\left( \frac{^{176}\text{Hf}}{^{177}\text{Hf}} \right)_{\text{CHUR}-ss} + \left( \frac{^{176}\text{Lu}}{^{177}\text{Hf}} \right)_{\text{CHUR}-p} (e^{\tilde{\lambda}_{176}t_{ss}} - e^{\tilde{\lambda}_{176}t})} - 1 \right] \times 10^4, \end{aligned} \quad (\text{S3})$$

where the quantities with the tilde accents take the same values as those without, but the difference is that the former have no error. This allows us to disentangle errors in  $\varepsilon^{176}\text{Hf}_{\text{zrc}-t,c/\text{CHUR}-t}$  arising from the CHUR determination from those arising from zircon analysis. This is most useful to evaluate the quality of the measurements independently of CHUR parameters from the literature. It also allows us to discuss model ages of KREEP extraction for zircon populations, treating each data point as independent. While this is not strictly correct because  $\lambda_{176}$  and  $t$  are present in both  $\varepsilon^{176}\text{Hf}_{\text{zrc}-t,c/\text{CHUR}-t}$  and  $\varepsilon^{176}\text{Hf}_{\text{zrc}-t,c/\text{CHUR}-t}$ , these terms are known well enough that they represent a very small portion of the overall uncertainty (2). We would not be able to consider zircon Hf isotopic analyses and their uncertainties as independent if the error of CHUR had been incorporated directly in  $\varepsilon^{176}\text{Hf}_{\text{zrc}-t,c/\text{CHUR}-t}$  following Eq. S2 (see Chen *et al.* (2) for details). We propagated the uncertainties on all parameters using approximate analytical equations that were verified against the results of Monte-Carlo simulations (2).

## 5. Calculation of model ages

We assume that the lunar magma ocean had a chondritic Lu/Hf ratio until the KREEP reservoir formed with a low Lu/Hf ratio, after which its  $^{176}\text{Hf}/^{177}\text{Hf}$  evolution diverged from that of CHUR. Zircons crystallized from the KREEP reservoir, either through protracted crystallization or more likely from large scale melting induced by basin-forming impacts (3). The initial  $^{176}\text{Hf}/^{177}\text{Hf}$  ratios of lunar zircons therefore record the temporal evolution of the  $^{176}\text{Hf}/^{177}\text{Hf}$  ratio in KREEP. We are interested in dating the time of this departure from CHUR, which we can obtain from zircons in two ways:

(i) We can use the initial  $^{176}\text{Hf}/^{177}\text{Hf}$  ratio and the age of a particular zircon and calculate backwards in time the  $^{176}\text{Hf}/^{177}\text{Hf}$  ratio of the KREEP reservoir that produced this zircon by assuming a  $^{176}\text{Lu}/^{177}\text{Hf}$  ratio for KREEP, and by examining when the model KREEP value crossed CHUR. A different model age  $t_d$  can be calculated for each zircon, the limitation being that we have to assume  $(^{176}\text{Lu}/^{177}\text{Hf})_{\text{KREEP}-p}$  (the present-day elemental ratio of the KREEP reservoir),

$$t_d = \frac{1}{\lambda_{176}} \ln \left[ e^{\lambda_{176}t} + \frac{(^{176}\text{Hf}/^{177}\text{Hf})_{\text{CHUR}-t} - (^{176}\text{Hf}/^{177}\text{Hf})_{\text{zrc}-t,c}}{(^{176}\text{Lu}/^{177}\text{Hf})_{\text{CHUR}-p} - (^{176}\text{Lu}/^{177}\text{Hf})_{\text{KREEP}-p}} \right], \quad (\text{S4})$$

where  $(^{176}\text{Hf}/^{177}\text{Hf})_{\text{CHUR}-t}$  and  $(^{176}\text{Hf}/^{177}\text{Hf})_{\text{zrc}-t,c}$  are the isotopic ratios of CHUR and the zircon (corrected for cosmogenic effects) at the time of zircon crystallization, respectively, while  $(^{176}\text{Lu}/^{177}\text{Hf})_{\text{CHUR}-p} - (^{176}\text{Lu}/^{177}\text{Hf})_{\text{KREEP}-p}$  are the elemental ratios of CHUR and KREEP at present. Previous studies gave estimates for  $(^{176}\text{Lu}/^{177}\text{Hf})_{\text{KREEP}-p}$  of 0.0164 (1),  $0.0154 \pm 0.0034$  (33), and  $0.00153 \pm 0.0033$  (34). The model ages of zircon calculated in this way are compiled in Datasets S1, assuming a constant  $(^{176}\text{Lu}/^{177}\text{Hf})_{\text{KREEP}-p} = 0.00153 \pm 0.0033$  (34). The uncertainties on the model ages  $t_d$  calculated using an approximate analytical equation that was verified against the result of a Monte-Carlo simulation (2) are also compiled in Datasets S1.

(ii) If all initial  $\varepsilon^{176}\text{Hf}$  values of zircons plot on a single line, this would be consistent with all of them crystallizing from KREEP with constant  $(^{176}\text{Lu}/^{177}\text{Hf})_{\text{KREEP}-p}$  that separated from CHUR at a

precisely defined time. In those circumstances  $\varepsilon^{176}\text{Hf}_{\text{zrc}-t,c}/\text{CHUR}-t$  of the zircon population should exhibit the following time-dependence,

$$\varepsilon^{176}\text{Hf}_{\text{zrc}-t,c} - \varepsilon^{176}\text{Hf}_{\text{CHUR}-t} = \frac{10^4[(^{176}\text{Lu}/^{177}\text{Hf})_{\text{KREEP}-p} - (^{176}\text{Lu}/^{177}\text{Hf})_{\text{CHUR}-p}](e^{\lambda_{176}t_d} - e^{\lambda_{176}t})}{(^{176}\text{Hf}/^{177}\text{Hf})_{\text{CHUR}-ss} + (^{176}\text{Lu}/^{177}\text{Hf})_{\text{CHUR}-p}(e^{\lambda_{176}t_{ss}} - e^{\lambda_{176}t})}. \quad (\text{S5})$$

This mathematical relationship is close to linear over the age span of the zircon grains analyzed, and our data indeed can be fit with a linear function, so we can safely use the following approximation at  $t_d$ ,

$$\varepsilon^{176}\text{Hf}_{\text{zrc}-t,c} - \varepsilon^{176}\text{Hf}_{\text{CHUR}-t} \simeq \varepsilon^{176}\text{Hf}_{\text{zrc}-t_d,c} - \varepsilon^{176}\text{Hf}_{\text{CHUR}-t_d} + \left. \frac{\partial(\varepsilon^{176}\text{Hf}_{\text{zrc}-t,c} - \varepsilon^{176}\text{Hf}_{\text{CHUR}-t})}{\partial t} \right|_{t=t_d} (t - t_d), \quad (\text{S6})$$

$$\varepsilon^{176}\text{Hf}_{\text{zrc}-t,c} - \varepsilon^{176}\text{Hf}_{\text{CHUR}-t} \simeq \left. \frac{\partial(\varepsilon^{176}\text{Hf}_{\text{zrc}-t,c} - \varepsilon^{176}\text{Hf}_{\text{CHUR}-t})}{\partial t} \right|_{t=t_d} (t - t_d), \quad (\text{S7})$$

$$\varepsilon^{176}\text{Hf}_{\text{zrc}-t,c} - \varepsilon^{176}\text{Hf}_{\text{CHUR}-t} \simeq \frac{10^4[(^{176}\text{Lu}/^{177}\text{Hf})_{\text{CHUR}-p} - (^{176}\text{Lu}/^{177}\text{Hf})_{\text{KREEP}-p}]}{(^{176}\text{Hf}/^{177}\text{Hf})_{\text{CHUR}-ss} + (^{176}\text{Lu}/^{177}\text{Hf})_{\text{CHUR}-p}(e^{\lambda_{176}t_{ss}} - e^{\lambda_{176}t_d})} \lambda_{176} (t - t_d), \quad (\text{S8})$$

$$\varepsilon^{176}\text{Hf}_{\text{zrc}-t,c} - \varepsilon^{176}\text{Hf}_{\text{CHUR}-t} \simeq 10^4[(^{176}\text{Lu}/^{177}\text{Hf})_{\text{CHUR}-p} - (^{176}\text{Lu}/^{177}\text{Hf})_{\text{KREEP}-p}][1 - (^{176}\text{Lu}/^{177}\text{Hf})_{\text{CHUR}-p} \lambda_{176} (t_{ss} - t_d)] \lambda_{176} (t - t_d). \quad (\text{S9})$$

The intercept with CHUR at  $\varepsilon^{176}\text{Hf}_{\text{zrc}-t,c} - \varepsilon^{176}\text{Hf}_{\text{CHUR}-t} = 0$  gives the age of KREEP  $t = t_d$ . The slope gives the  $(^{176}\text{Lu}/^{177}\text{Hf})_{\text{KREEP}-p}$  ratio. If we write  $s$  the value of the slope in a diagram  $\varepsilon^{176}\text{Hf}_{\text{zrc}-t,c} - \varepsilon^{176}\text{Hf}_{\text{CHUR}-t}$  vs.  $t$ , we indeed have,

$$(^{176}\text{Lu}/^{177}\text{Hf})_{\text{KREEP}-p} \simeq (^{176}\text{Lu}/^{177}\text{Hf})_{\text{CHUR}-p} - 10^{-4}s(1/\lambda_{176} + t_{ss} - t_d). \quad (\text{S10})$$

A virtue of this approach is that the  $^{176}\text{Lu}/^{177}\text{Hf}$  ratio of KREEP is calculated from the zircon data rather than assumed based on literature data. The caveat is that it only works if KREEP had a relatively simple history, but this assumption can be tested by evaluating the quality of the linear regression, as any departure from a line will indicate either that KREEP was not isolated at a single time, or its  $^{176}\text{Lu}/^{177}\text{Hf}$  ratio varied spatially or temporally.

To find the model age and  $^{176}\text{Lu}/^{177}\text{Hf}$  of KREEP, we fit  $\varepsilon^{176}\text{Hf}_{\text{zrc}-t,c} - \varepsilon^{176}\text{Hf}_{\text{CHUR}-t}$  and  $t$  with a line to calculate its intercept with the  $x$ -axis and its slope. We calculated the MSWD and the data can indeed be fit by a line. Because the CHUR baseline is not independent for all  $\varepsilon^{176}\text{Hf}_{\text{zrc}-t,c}$  values, the uncertainty on the model age of KREEP is more accurately calculated by using a Monte Carlo simulation (MCS) (2). Best-fit lines and CHUR baselines were generated following prescribed distributions for the data points and CHUR parameters, and the slopes and intercepts were calculated (2). The intercept ensemble can be described using a binormal distribution that we calculated. We are mostly interested in the marginal probability distribution of  $t_d$ , which we also calculated and is the basis for our uncertainty estimate. We use the mode of the marginal probability distribution of  $t_d$  as best estimate and calculate its 95% confidence interval by taking the 0.025-0.975 interquantile range.

## 6. Comparison between leachate (L2) and residue (R) $^{176}\text{Hf}/^{177}\text{Hf}$ initial values

For zircons for which we have measured both leachate (L2) and residue (R), we are interested in understanding what causes the corrected initial  $^{176}\text{Hf}/^{177}\text{Hf}$  values to sometimes differ. The differences between leachate and residue are in all cases small and we can study the cause for the discrepancy by writing the leachate value as a perturbation from the residue value,

$$\varepsilon^{176}\text{Hf}_{\text{L}-t,c}/\text{CHUR}-t \simeq \varepsilon^{176}\text{Hf}_{\text{R}-t,c} + \frac{\partial \varepsilon^{176}\text{Hf}_{\text{R}}}{\partial (^{176}\text{Hf}/^{177}\text{Hf})_{\text{zrc}-p}} ( (^{176}\text{Hf}/^{177}\text{Hf})_{\text{L}-p} - (^{176}\text{Hf}/^{177}\text{Hf})_{\text{R}-p} ) + \frac{\partial \varepsilon^{176}\text{Hf}_{\text{R}}}{\partial \varepsilon^i\text{Hf}} (\varepsilon^i\text{Hf}_{\text{L}} - \varepsilon^i\text{Hf}_{\text{R}}) + \frac{\partial \varepsilon^{176}\text{Hf}_{\text{R}}}{\partial (^{176}\text{Lu}/^{177}\text{Hf})_{\text{zrc}-p}} ( (^{176}\text{Lu}/^{177}\text{Hf})_{\text{L}} - (^{176}\text{Lu}/^{177}\text{Hf})_{\text{R}} ) + \frac{\partial \varepsilon^{176}\text{Hf}_{\text{R}}}{\partial e^{\lambda_{176}t}} (e^{\lambda_{176}t_{\text{L}}} - e^{\lambda_{176}t_{\text{R}}}). \quad (\text{S11})$$

After calculating the partial derivatives and removing the negligible terms, we have,

$$\varepsilon^{176}\text{Hf}_{\text{L}-t,c} - \varepsilon^{176}\text{Hf}_{\text{R}-t,c} \simeq (\varepsilon^{176}\text{Hf}_{\text{L}-p} - \varepsilon^{176}\text{Hf}_{\text{R}-p}) - \alpha_i (\varepsilon^i\text{Hf}_{\text{L}} - \varepsilon^i\text{Hf}_{\text{R}}) + \frac{10^4(1 - e^{\lambda_{176}t})}{^{176}\text{Hf}/^{177}\text{Hf}_{\text{CHUR}-t}} ( (^{176}\text{Lu}/^{177}\text{Hf})_{\text{L}} - (^{176}\text{Lu}/^{177}\text{Hf})_{\text{R}} ) + 10^4 \frac{(^{176}\text{Lu}/^{177}\text{Hf})_{\text{CHUR}-p} - (^{176}\text{Lu}/^{177}\text{Hf})_{\text{zrc}-p}}{^{176}\text{Hf}/^{177}\text{Hf}_{\text{CHUR}-t}} (e^{\lambda_{176}t_{\text{L}}} - e^{\lambda_{176}t_{\text{R}}}). \quad (\text{S12})$$

where  $\epsilon^{176}\text{Hf}_{\text{L-p}}$  and  $\epsilon^{176}\text{Hf}_{\text{R-p}}$  are measured values reported relative to the JMC 475 standard solution. We plot in Fig. S2 the contributions of each term to the overall difference in  $^{176}\text{Hf}/^{177}\text{Hf}$  initial values between leachates and residues.

Zircons can undergo various transformations after formation, including Pb-loss and multi-phase growth (35). Utilizing zircons with these complex histories can lead to data that are difficult to interpret. Additionally, fractionation of the Lu/Hf ratio during chemical abrasion may produce inaccurate initial  $\epsilon^{176}\text{Hf}$  values (2). To mitigate these issues, we have classified the data into three tiers of reliability. This stratification allows us to filter out disturbed zircons, while maintaining enough original data to yield statistically significant insights into Lu-Hf model ages.

- *Tier 1*: The most reliable indicator of zircon data integrity, reflecting a straightforward history unaffected by laboratory processing, is when L2 and R exhibit similar ages and initial  $\epsilon^{176}\text{Hf}$  values. We have identified 9 zircons meeting these criteria: 14311\_58 z8, 14311\_58 z12, 14311\_58 z34, 14311\_58 z40, 14311\_58 z59, 14311\_58 z61, 14163\_65 z4 (this study), 14311\_58 z37 (Barboni *et al.* (36)), and 72275A z1 (Chen *et al.* (2)), comprising 18 U-Pb ages and initial  $\epsilon^{176}\text{Hf}$  values.
- *Tier 2*: Figure S2 illustrates that in most instances where the initial corrected  $\epsilon^{176}\text{Hf}$  values differ between L2 and R, the raw  $\epsilon^{176}\text{Hf}$  values agree. This discrepancy is often due to significant and varying Lu/Hf ratios. It is highly unlikely for different domains within a single zircon to have originated with distinct initial  $\epsilon^{176}\text{Hf}$  values and Lu/Hf ratios, and then fortuitously converge to similar present-day  $\epsilon^{176}\text{Hf}$  values after  $^{176}\text{Lu}$  decay. The different initial corrected  $\epsilon^{176}\text{Hf}$  values are most likely an analytical artifact from fractionation of the Lu/Hf ratio during processing. Chemical abrasion and leaching, intended to remove domains susceptible to Pb-loss, could have caused this fractionation. The residues are most resistant and least affected by Pb-loss. They also contain the majority of Lu and Hf released during chemical abrasion (Table S1). They are therefore likely to retain undisturbed Lu/Hf ratios. In addition to all *Tier 1* measurements, we include in *Tier 2* the residue values with consistent measured (raw)  $\epsilon^{176}\text{Hf}$  values between leachate and residue. Along with the *Tier 1* zircons, we have identified 9 additional zircons meeting *Tier 2* criteria: 14311\_58-z57, 14311\_58-z18, 14311\_58-z15, 14311\_58-z47, 14311\_58-z6, 14311\_58-z27, 14163\_949-z3 (this study), 15405\_75-z1 and 14163\_65-z7 (Barboni *et al.* (36)). *Tier 2* thus encompasses 27 data points, including 18 from *Tier 1* and 9 additional residue (R) values.
- *Tier 3*: In some instances, insufficient Hf was available to measure L2. All zircons were selected via cathodoluminescence imaging for their probable simple histories (3). Typically, residues, which hold the majority of Lu and Hf, should be less affected by Lu/Hf fractionation during dissolution. Our third approach includes the 27 data points from *Tier 2*, adding the following residues (R): 14311\_58-z9, 14311\_58-z7, 14311\_58-z21, 14311\_58-z38, 14311\_58-z69a, 14311\_58-z69b, 14311\_58-z71, 14311\_58-z14, 14311\_58-z64, 14311\_58-z58, 14311\_58-z60, 14311\_58-z24 (this study), and 14163A-z89 (Chen *et al.* (2)). This corresponds to 13 residue measurements, on top of the 27 counted in *Tier 2*, for a total of 40 data points.

We treat all data as independent in calculation of the number of degrees of freedom and confidence intervals. In reality, because L2 and R are measured on the same zircon, those paired data are correlated to some extent. To assess this effect, we have also performed regressions by calculating the weighted mean and uncertainty for each pair and use these values in the regressions (Fig. S3). The conclusion of this analysis is that L2-R pairing affects minimally the results.

## 7. Comparison with model $^{146}\text{Sm}$ - $^{142}\text{Nd}$ and $^{147}\text{Sm}$ - $^{143}\text{Nd}$ model ages of mare basalt source formation

A significant argument for a Moon formed relatively late at  $\sim 4.33$  Ga has been made based on Nd isotopic analyses of KREEP-free mare basalts that provide a  $^{146}\text{Sm}$ - $^{142}\text{Nd}$ - $^{147}\text{Sm}$ - $^{143}\text{Nd}$  model age for the formation of the ultramafic cumulate lithologies that produced the mare basalts (37, 38). Because those data contradict the age that we infer for KREEP, we examine below the assumptions and observations that support such a young age, focusing on the high-quality extensive dataset of Borg *et al.* (37).

We consider a 2-stage model. Time is expressed backwards relative to present, so the solar system formed at  $t_{\text{ss}} = 4.567$  Ga. The Sm/Nd ratio follows a chondritic (CHUR) evolution from the time of solar system formation  $t_{\text{ss}}$  to the time of lunar magma ocean crystallization and formation of ultramafic cumulate lithologies  $t_{\text{LMO}}$ . The Sm/Nd ratio is then fractionated by crystallization of the lunar magma and formation

of mafic cumulate lithologies, which we write  $(\text{Sm}/\text{Nd})_{\text{UMC}}$ . Upon melting of ultramafic cumulate lithologies, mare basalts are formed at time  $t_{\text{MB}}$  and the Sm/Nd ratio is further fractionated relative to the source. All Sm/Nd ratios are expressed at the present time  $t_p$ . We are interested in tracking ingrowth of  $^{142}\text{Nd}$  and  $^{143}\text{Nd}$  resulting from decay of  $^{146}\text{Sm}$  ( $\lambda_{146} = 6.73 \pm 0.33 \times 10^{-9} \text{ yr}^{-1}$ ;  $t_{1/2} = 103 \pm 5 \text{ Myr}$  (37, 39)) and  $^{147}\text{Sm}$  ( $\lambda_{147} = 6.539 \times 10^{-12} \text{ yr}^{-1}$ ;  $t_{1/2} = 106 \text{ Gyr}$ ). The equations are very similar for the two decay systems, and we use  $i$  and  $j$  to denote parent and decay product (as in  $^i\text{Sm}$  and  $^j\text{Nd}$ ).

Between  $t_{\text{ss}}$  and  $t_{\text{LMO}}$ , the Sm/Nd follows a chondritic evolution,

$$\left(\frac{^j\text{Nd}}{^{144}\text{Nd}}\right)_{\text{UMC}, t_{\text{LMO}}} = \left(\frac{^j\text{Nd}}{^{144}\text{Nd}}\right)_{\text{CHUR}, t_{\text{ss}}} + \left(\frac{^i\text{Sm}}{^{144}\text{Nd}}\right)_{\text{CHUR}, t_{\text{ss}}} [1 - e^{-\lambda_i(t_{\text{ss}} - t_{\text{LMO}})}], \quad (\text{S13})$$

$$\left(\frac{^j\text{Nd}}{^{144}\text{Nd}}\right)_{\text{UMC}, t_{\text{LMO}}} = \left(\frac{^j\text{Nd}}{^{144}\text{Nd}}\right)_{\text{CHUR}, t_{\text{ss}}} + \left(\frac{^i\text{Sm}}{^{147}\text{Sm}}\right)_{\text{CHUR}, t_{\text{ss}}} \left(\frac{^{147}\text{Sm}}{^{144}\text{Nd}}\right)_{\text{CHUR}, t_{\text{ss}}} [1 - e^{-\lambda_i(t_{\text{ss}} - t_{\text{LMO}})}], \quad (\text{S14})$$

$$\left(\frac{^j\text{Nd}}{^{144}\text{Nd}}\right)_{\text{UMC}, t_{\text{LMO}}} = \left(\frac{^j\text{Nd}}{^{144}\text{Nd}}\right)_{\text{CHUR}, t_{\text{ss}}} + \left(\frac{^i\text{Sm}}{^{147}\text{Sm}}\right)_{\text{CHUR}, t_{\text{ss}}} \left(\frac{^{147}\text{Sm}}{^{144}\text{Nd}}\right)_{\text{CHUR}, t_p} e^{\lambda_{147} t_{\text{ss}}} [1 - e^{-\lambda_i(t_{\text{ss}} - t_{\text{LMO}})}], \quad (\text{S15})$$

where  $(^j\text{Nd}/^{144}\text{Nd})_{\text{CHUR}, t_{\text{ss}}}$  is the initial CHUR ratio at solar system formation,  $(^i\text{Sm}/^{147}\text{Sm})_{t_{\text{ss}}}$  is the initial solar system ratio, and  $(^{147}\text{Sm}/^{144}\text{Nd})_{\text{CHUR}, t_p}$  is the present day CHUR ratio ( $t_p = 0 \text{ Ga}$  in our time reference).

To make the comparison easier, we use the same model parameters as Borg *et al.* (37) whenever possible. We use  $(^{143}\text{Nd}/^{144}\text{Nd})_{\text{CHUR}, t_{\text{ss}}} = 0.506674$ ,  $(^{147}\text{Sm}/^{144}\text{Nd})_{\text{CHUR}, t_p} = 0.1967$ , and  $(^{146}\text{Sm}/^{147}\text{Sm})_{t_{\text{ss}}} = 0.00164 \pm 0.00009$  [combining  $(^{146}\text{Sm}/^{144}\text{Sm})_{t_{\text{ss}}} = 0.00828 \pm 0.00044$  (39) and  $(^{147}\text{Sm}/^{144}\text{Sm})_{t_{\text{ss}}} = 5.04$  (37)]. In CHUR, we have,

$$\left(\frac{^j\text{Nd}}{^{144}\text{Nd}}\right)_{\text{CHUR}, t_{\text{ss}}} = \left(\frac{^j\text{Nd}}{^{144}\text{Nd}}\right)_{\text{CHUR}, t_p} - \left(\frac{^i\text{Sm}}{^{147}\text{Sm}}\right)_{\text{CHUR}, t_{\text{ss}}} \left(\frac{^{147}\text{Sm}}{^{144}\text{Nd}}\right)_{\text{CHUR}, t_p} e^{\lambda_{147} t_{\text{ss}}} (1 - e^{-\lambda_i t_{\text{ss}}}). \quad (\text{S16})$$

We can use the terrestrial standard  $^{142}\text{Nd}/^{144}\text{Nd}$  ratio of 1.141837 (40) as a proxy for the present-day CHUR (BSE) ratio to calculate  $(^j\text{Nd}/^{144}\text{Nd})_{\text{CHUR}, t_{\text{ss}}} = 1.141503$ . This is close to previously proposed values of 1.14160 $\pm$ 0.00011 (41) and 1.141479 $\pm$ 0.000013 (42). Given the possible nucleosynthetic heterogeneity in the Nd isotopic composition of the solar system (43), we prefer to rely on measurements of the terrestrial Nd isotopic composition to estimate  $(^j\text{Nd}/^{144}\text{Nd})_{\text{CHUR}, t_{\text{ss}}}$  relevant to lunar differentiation. This is a significant source of uncertainty in model ages of lunar magma ocean crystallization based on Nd isotopic analyses of individual mare basalts. As discussed below, using several mare basalt measurements together provides a way to minimize this influence. In the second stage between formation of ultramafic cumulate lithologies and mare basalt formation, we have,

$$\left(\frac{^j\text{Nd}}{^{144}\text{Nd}}\right)_{\text{MB}, t_{\text{MB}}} = \left(\frac{^j\text{Nd}}{^{144}\text{Nd}}\right)_{\text{UMC}, t_{\text{LMO}}} + \left(\frac{^i\text{Sm}}{^{144}\text{Nd}}\right)_{\text{UMC}, t_{\text{LMO}}} [1 - e^{-\lambda_i(t_{\text{LMO}} - t_{\text{MB}})}], \quad (\text{S17})$$

$$\left(\frac{^j\text{Nd}}{^{144}\text{Nd}}\right)_{\text{MB}, t_{\text{MB}}} = \left(\frac{^j\text{Nd}}{^{144}\text{Nd}}\right)_{\text{UMC}, t_{\text{LMO}}} + \left(\frac{^i\text{Sm}}{^{147}\text{Sm}}\right)_{\text{CHUR}, t_{\text{ss}}} \left(\frac{^{147}\text{Sm}}{^{144}\text{Nd}}\right)_{\text{UMC}, t_p} e^{\lambda_{147} t_{\text{ss}}} [e^{-\lambda_i(t_{\text{ss}} - t_{\text{LMO}})} - e^{-\lambda_i(t_{\text{ss}} - t_{\text{MB}})}]. \quad (\text{S18})$$

By introducing Eq. S15 into this relationship, we obtain,

$$\begin{aligned} \left(\frac{^j\text{Nd}}{^{144}\text{Nd}}\right)_{\text{MB}, t_{\text{MB}}} &= \left(\frac{^j\text{Nd}}{^{144}\text{Nd}}\right)_{\text{CHUR}, t_{\text{ss}}} + \left(\frac{^i\text{Sm}}{^{147}\text{Sm}}\right)_{\text{CHUR}, t_{\text{ss}}} \left(\frac{^{147}\text{Sm}}{^{144}\text{Nd}}\right)_{\text{CHUR}, t_p} e^{\lambda_{147} t_{\text{ss}}} [1 - e^{-\lambda_i(t_{\text{ss}} - t_{\text{LMO}})}] + \\ &\quad \left(\frac{^i\text{Sm}}{^{147}\text{Sm}}\right)_{\text{CHUR}, t_{\text{ss}}} \left(\frac{^{147}\text{Sm}}{^{144}\text{Nd}}\right)_{\text{UMC}, t_p} e^{\lambda_{147} t_{\text{ss}}} [e^{-\lambda_i(t_{\text{ss}} - t_{\text{LMO}})} - e^{-\lambda_i(t_{\text{ss}} - t_{\text{MB}})}]. \end{aligned} \quad (\text{S19})$$

We can write this equation for the two decay systems,

$$\begin{aligned} \left(\frac{^{142}\text{Nd}}{^{144}\text{Nd}}\right)_{\text{MB}, t_{\text{MB}}} &= \left(\frac{^{142}\text{Nd}}{^{144}\text{Nd}}\right)_{\text{CHUR}, t_{\text{ss}}} + \left(\frac{^{146}\text{Sm}}{^{147}\text{Sm}}\right)_{\text{CHUR}, t_{\text{ss}}} \left(\frac{^{147}\text{Sm}}{^{144}\text{Nd}}\right)_{\text{CHUR}, t_p} e^{\lambda_{147} t_{\text{ss}}} [1 - e^{-\lambda_{146}(t_{\text{ss}} - t_{\text{LMO}})}] + \\ &\quad \left(\frac{^{146}\text{Sm}}{^{147}\text{Sm}}\right)_{\text{CHUR}, t_{\text{ss}}} \left(\frac{^{147}\text{Sm}}{^{144}\text{Nd}}\right)_{\text{UMC}, t_p} e^{\lambda_{147} t_{\text{ss}}} [e^{-\lambda_{146}(t_{\text{ss}} - t_{\text{LMO}})} - e^{-\lambda_{146}(t_{\text{ss}} - t_{\text{MB}})}], \end{aligned} \quad (\text{S20})$$

$$\begin{aligned} \left(\frac{^{143}\text{Nd}}{^{144}\text{Nd}}\right)_{\text{MB}, t_{\text{MB}}} &= \left(\frac{^{143}\text{Nd}}{^{144}\text{Nd}}\right)_{\text{CHUR}, t_{\text{ss}}} + \left(\frac{^{147}\text{Sm}}{^{144}\text{Nd}}\right)_{\text{CHUR}, t_p} (e^{\lambda_{147} t_{\text{ss}}} - e^{\lambda_{147} t_{\text{LMO}}}) + \left(\frac{^{147}\text{Sm}}{^{144}\text{Nd}}\right)_{\text{UMC}, t_p} (e^{\lambda_{147} t_{\text{LMO}}} - \\ &\quad e^{\lambda_{147} t_{\text{MB}}}). \end{aligned} \quad (\text{S21})$$

We are interested in relating  $^{142}\text{Nd}$  excesses to the Sm/Nd ratio for the source material of mare basalts. The Sm/Nd ratio can be fractionated during melting and fractional crystallization, but its value in the source can



be indirectly inferred from  $^{143}\text{Nd}$  excesses. To do that, we eliminate  $(^{147}\text{Sm}/^{144}\text{Nd})_{UMC,t_p}$  from the two equations above, and we obtain,

$$\begin{aligned} \left(\frac{^{142}\text{Nd}}{^{144}\text{Nd}}\right)_{MB,t_{MB}} &= \left(\frac{^{142}\text{Nd}}{^{144}\text{Nd}}\right)_{CHUR,t_{ss}} + \left(\frac{^{146}\text{Sm}}{^{147}\text{Sm}}\right)_{CHUR,t_{ss}} \left(\frac{^{147}\text{Sm}}{^{144}\text{Nd}}\right)_{CHUR,t_p} e^{\lambda_{147}t_{ss}} [1 - e^{-\lambda_{146}(t_{ss}-t_{LMO})}] + \\ &\quad \left(\frac{^{146}\text{Sm}}{^{147}\text{Sm}}\right)_{CHUR,t_{ss}} \left[ \left(\frac{^{143}\text{Nd}}{^{144}\text{Nd}}\right)_{MB,t_{MB}} - \left(\frac{^{143}\text{Nd}}{^{144}\text{Nd}}\right)_{CHUR,t_{ss}} - \left(\frac{^{147}\text{Sm}}{^{144}\text{Nd}}\right)_{CHUR,t_p} (e^{\lambda_{147}t_{ss}} - \right. \\ &\quad \left. e^{\lambda_{147}t_{LMO}}) \right] \left( \frac{e^{\lambda_{146}t_{LMO}} - e^{\lambda_{146}t_{MB}}}{e^{\lambda_{147}t_{LMO}} - e^{\lambda_{147}t_{MB}}} \right) e^{(\lambda_{147}-\lambda_{146})t_{ss}}. \end{aligned} \quad (\text{S22})$$

In CHUR, we have,

$$\left(\frac{^{142}\text{Nd}}{^{144}\text{Nd}}\right)_{CHUR,t_p} = \left(\frac{^{142}\text{Nd}}{^{144}\text{Nd}}\right)_{CHUR,t_{ss}} + \left(\frac{^{146}\text{Sm}}{^{147}\text{Sm}}\right)_{CHUR,t_{ss}} \left(\frac{^{147}\text{Sm}}{^{144}\text{Nd}}\right)_{CHUR,t_p} e^{\lambda_{147}t_{ss}} (1 - e^{-\lambda_{146}t_{ss}}). \quad (\text{S23})$$

For a given mare basalt, Sm-Nd isochrons yield initial Nd isotopic compositions  $\varepsilon^{142}\text{Nd}_{MB,t_{MB}}$  and  $\varepsilon^{143}\text{Nd}_{MB,t_{MB}}$ , as well as the age  $t_{MB}$ . We can thus calculate a model age of LMO differentiation  $t_{LMO}$  by solving the above equation for this unknown. Sometimes, only bulk Nd isotopic composition, Sm/Nd, and age are reported. In those cases, the following formula can be used to calculate initial Nd isotopic compositions at the time of mare basalt crystallization,

$$\left(\frac{^{142}\text{Nd}}{^{144}\text{Nd}}\right)_{MB,t_{MB}} = \left(\frac{^{142}\text{Nd}}{^{144}\text{Nd}}\right)_{MB,t_p} - \left(\frac{^{146}\text{Sm}}{^{147}\text{Sm}}\right)_{t_{ss}} \left(\frac{^{147}\text{Sm}}{^{144}\text{Nd}}\right)_{MB,t_p} e^{\lambda_{147}t_{ss}} [e^{-\lambda_{146}(t_{ss}-t_{MB})} - e^{-\lambda_{146}t_{ss}}]. \quad (\text{S24})$$

Several studies have reported mare basalt Nd isotopic compositions (37, 44-46). The data considered here are from Borg *et al.* (37), as these were all measured using the same protocol and show less dispersion than other data sets (38). Borg *et al.* (37) reported a model age for the source of non-KREEP mare basalts of  $4.336 \pm 0.030$  Myr, which was subsequently revised to  $4.331 \pm 0.014$  Myr (38). We plot in Fig. S5 the predicted  $^{142}\text{Nd}/^{144}\text{Nd}$  initial ratios of mare basalts (at the time of eruption/solidification) with the measured  $^{142}\text{Nd}/^{144}\text{Nd}$  initial ratios. The predicted  $^{142}\text{Nd}/^{144}\text{Nd}$  initial ratios are calculated based on  $^{143}\text{Nd}/^{144}\text{Nd}$  initial ratios measured in the same samples. We leave the CHUR (bulk silicate Moon)  $^{142}\text{Nd}/^{144}\text{Nd}$  initial ratio and time of LMO differentiation as adjustable parameters. As expected, we confirm the finding of Borg and Carlson (38) and references therein that the Nd isotopic data are best explained by an age of 4.33 Ga. All data cannot however be explained by a single age. We also plot the predicted  $^{142}\text{Nd}/^{144}\text{Nd}$  mare basalt initial values for an age of LMO differentiation of 4.44 Ga. The match between observed and predicted values is not as good as with a model age of 4.33 Ga.

To summarize, we agree that the model age for the source of mare basalts that best fits the data is 4.33 Ga, but many data are unexplained indicating incomplete resetting. As discussed in the main text, this age could reflect incipient melting or density-driven mixing among the cumulate lithologies that would later form the mare basalts.

## 8. Zircon saturation in KREEP magma

The zircons analyzed are from regolith lithologies and lack petrologic context. Some of them could have crystallized from KREEP-rich basalts erupted at the lunar surface, while others could have formed by cooling of the KREEP magma reservoir (47). In Fig. S6, we calculate the degree of crystallization and temperature at which zircons would crystallize from a KREEP magma (48) using the MELTS model (49) and a zircon saturation model (50). Under this simplistic scenario, it would take 88% crystallization for the magma to reach saturation. This means that the lunar magma ocean could have reached 99.9% crystallization before lunar zircons started crystallizing (99% to make KREEP, and 90% crystallization of the 1% remaining KREEP magma to saturate zircons). LMO crystallization is not the only event that could have formed zircons. Crystallization of erupted lavas rich in KREEP and secondary melting by impacts could have played significant roles as well.

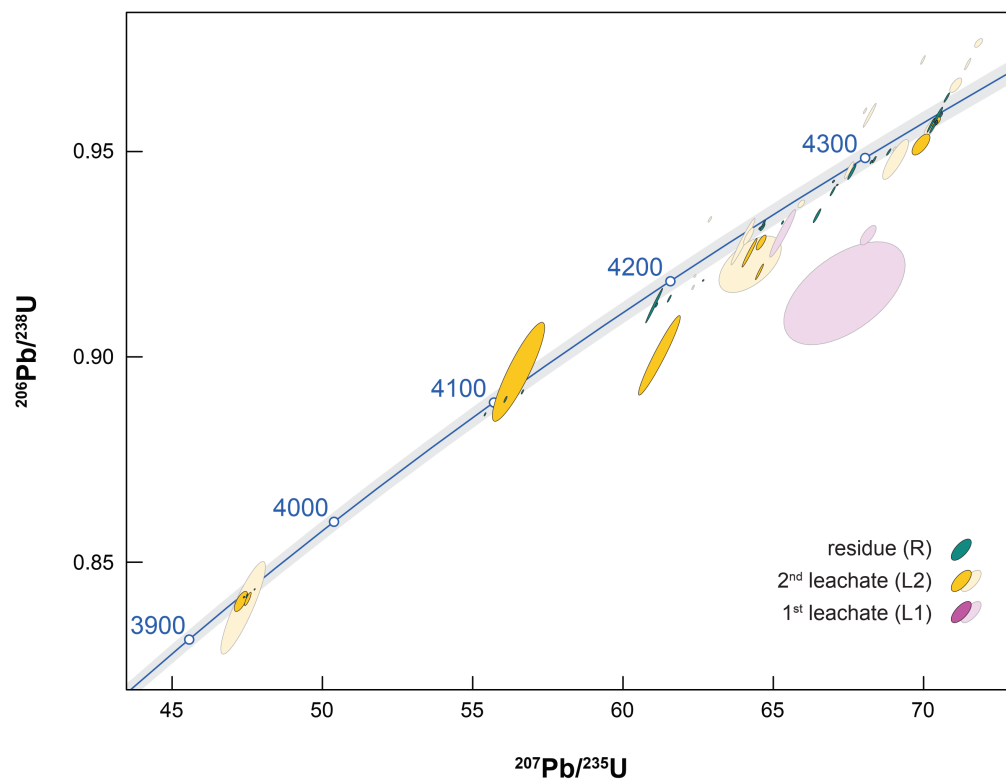


**Fig. S1.** Wetherill concordia diagram of all U–Pb ID-TIMS zircon dates (3) used to determine Hf model ages in this study, separated into residue (R), second leachate (L2) and first leachate (L1) aliquots. Leachates and residues classified as Tier 1, 2, and 3 are depicted in solid colors, whereas other leachates are shown in transparent colors.

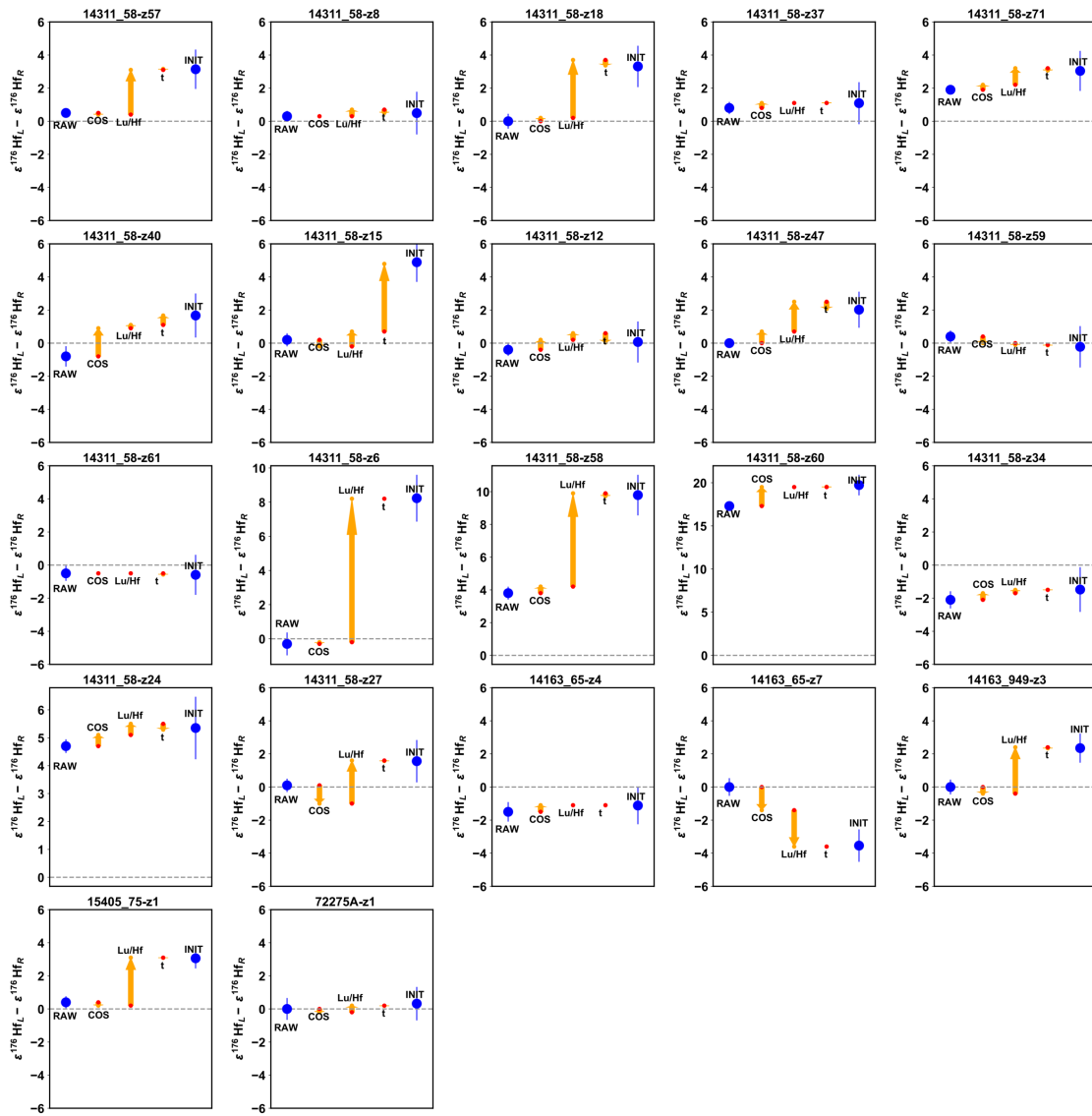


**Fig. S2.** Analysis of the origin of the difference in initial  $\varepsilon^{176}\text{Hf}$  values between leachate and residue based on Eq. S12. Each panel corresponds to a different zircon for which L2 and R data are available (the name of each zircon is indicated at the top of each panel). The blue filled dot on the left of each panel is the measured (RAW) isotopic difference between leachate and residue  $\varepsilon^{176}\text{Hf}_{\text{L-p}} - \varepsilon^{176}\text{Hf}_{\text{R-p}}$ . Each yellow arrow indicates how differences in the correction of cosmogenic effects (COS), parent/product ratio ( $^{176}\text{Lu}/^{177}\text{Hf}$ ), time (t) influence the overall difference in initial  $\varepsilon^{176}\text{Hf}$  values after correction of cosmogenic effects and in situ  $^{176}\text{Lu}$ -decay. The difference in initial corrected  $\varepsilon^{176}\text{Hf}$  values between leachate and residue is shown as a blue filled dot on the right of each panel (INIT).

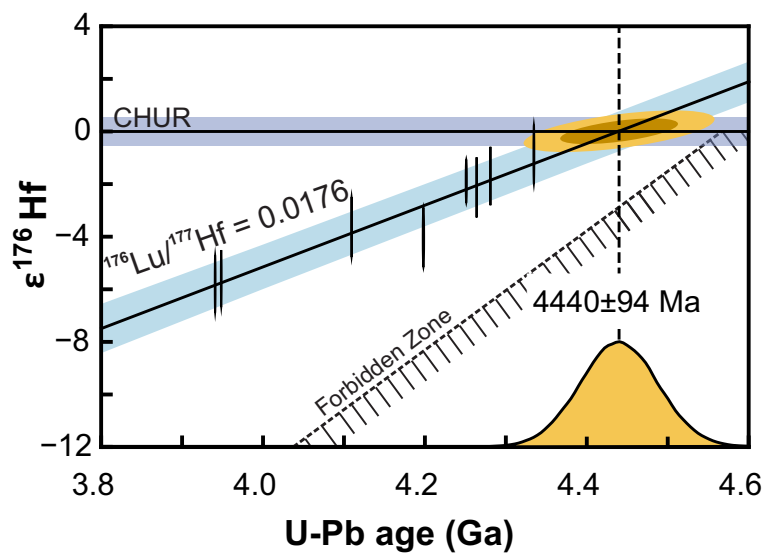


**Fig. S3.** Weighted mean initial  $\epsilon^{176}\text{Hf}$  values (cosmogenic effects were corrected using  $\epsilon^{178}\text{Hf}$ ) and U/Pb ages of leachates L2 and residues for Tier 1 lunar zircons.

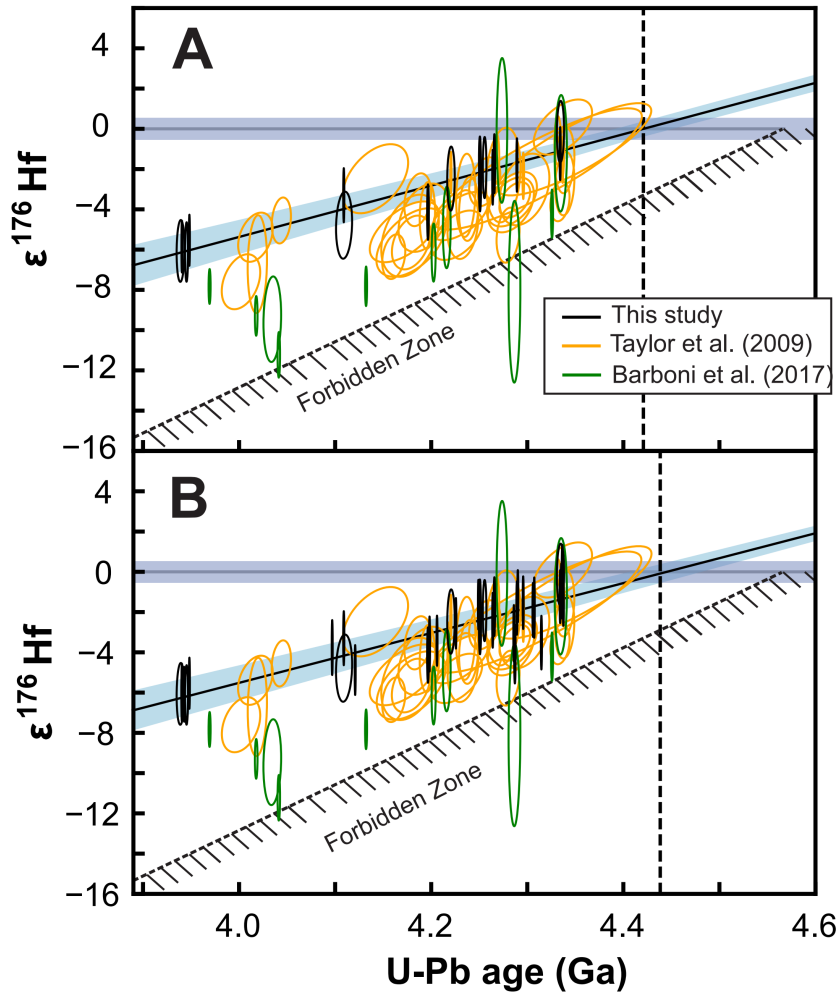


**Fig. S4.** Comparison between present analyses of initial  $\epsilon^{176}\text{Hf}$  values (cosmogenic effects were corrected using  $\epsilon^{178}\text{Hf}$ ) and U-Pb ages of lunar zircons (Table S1) and previous studies (1, 22). The top panel (A) shows Tier 1 data, while the bottom panel (B) shows Tier 3 data. As illustrated, the new data are significantly more precise and show significantly less scatter than previous data.

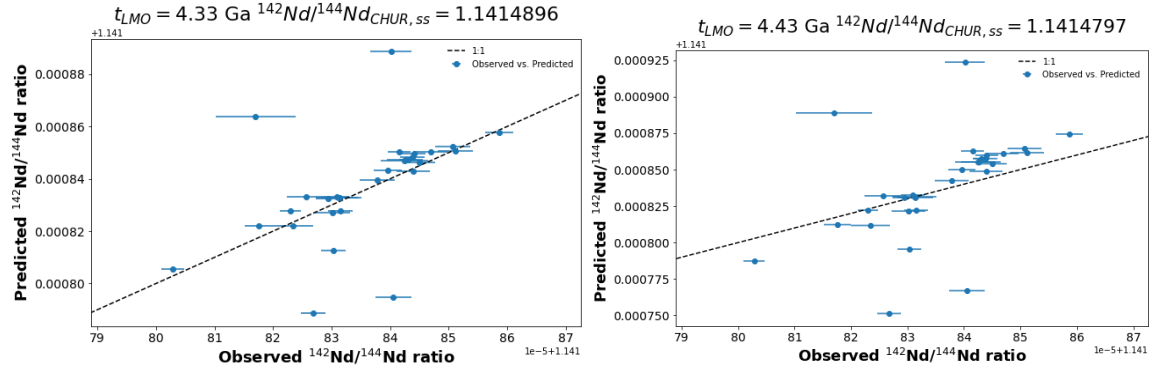


**Fig. S5.** Comparison between predicted and observed  $^{142}\text{Nd}/^{144}\text{Nd}$  initial ratios of mare basalts using a 2-stage model (Eq. S22) for different model ages of LMO crystallization (4.33 Ga on the left (38); 4.43 Ga on the right; this study). In each case, the CHUR (bulk silicate Moon)  $^{142}\text{Nd}/^{144}\text{Nd}$  initial ratio at the time of solar system formation was adjusted to fit the data. The predicted mare basalt  $^{142}\text{Nd}/^{144}\text{Nd}$  initial ratios were calculated using measured  $^{143}\text{Nd}/^{144}\text{Nd}$  initial ratios. Data from Borg *et al.* (37).

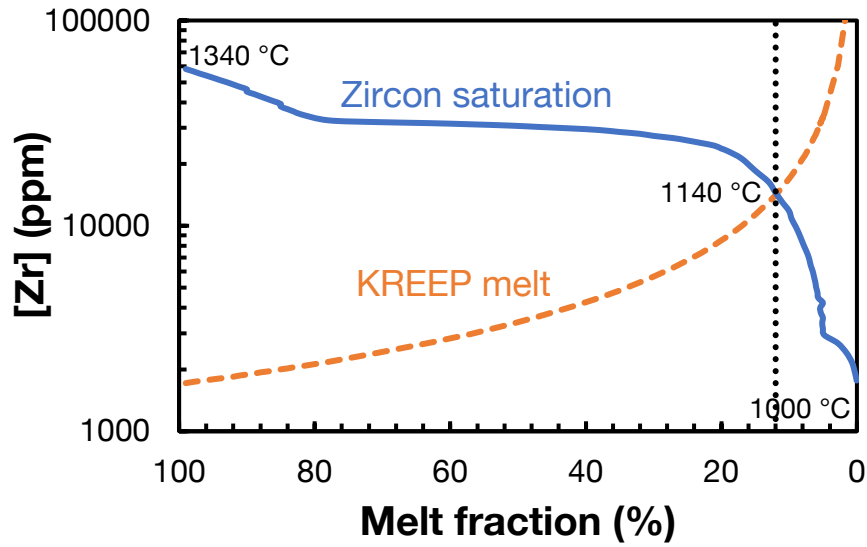


**Fig. S6.** Calculation of zircon saturation in a KREEP magma during equilibrium crystallization. The blue solid curve is the zircon saturation curve (50) for equilibrium crystallization of anhydrous bulk KREEP composition (48) at 5 kbar based on the MELTS model (49). The KREEP melt curve assumes complete incompatible behavior of Zr, starting with the Zr concentration of KREEP from Warren and Wasson (48). As shown, crystallizing KREEP liquid will not saturate zircon until the melt is 88% crystallized (melt fraction=12 %) at 1140 °C.

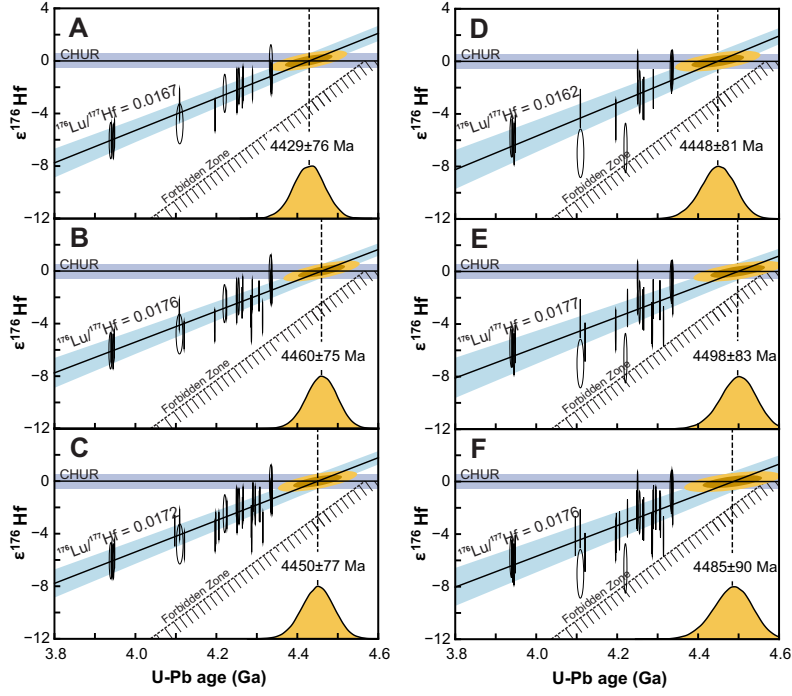


**Fig. S7.** Comparison between Tier 1 (A, D), Tier 2 (B, E) and Tier 3 (C, F) data sets correcting cosmogenic effects either using  $\epsilon^{178}\text{Hf}$  (A, B, C) or  $\epsilon^{180}\text{Hf}$  (D, E, F). Details on the latter correction are provided in the text and Chen *et al.* (2). As shown, all KREEP model ages and  $^{176}\text{Lu}/^{177}\text{Hf}$  ratios inferred from the data agree. Correction using  $\epsilon^{180}\text{Hf}$  introduces some scatter, the origin of which is uncertain.



**Table S1.** Summary of U-Pb ages and Hf isotopic compositions of lunar zircons

| Sample          | Tier # | Hf<br>(ng) | Zircon<br>diameter<br>( $\mu\text{m}$ ) | $\epsilon^{176}\text{Hf}_{\text{CHUR}}$<br>corrected<br>with $^{178}\text{Hf}$ | $2\sigma^*$ | $\epsilon^{176}\text{Hf}_{\text{CHUR}}$<br>corrected<br>with $^{180}\text{Hf}$ | $2\sigma^*$ | Lu/Hf<br>(ppm/ppm) | $2\sigma$ | Pb-Pb<br>Ages<br>(Ma) <sup>a</sup> | $2\sigma$ | Ref<br>(Ages) | Ref<br>( $\epsilon^{176}\text{Hf}$ ) |
|-----------------|--------|------------|---|--|-------------|--|-------------|--------------------|-----------|------------------------------------|-----------|---------------|--------------------------------------|
| 14311_58_z8_R   | 1,2,3  | 17.4       | 90                                      | -2.41  | 1.36        | -2.90  | 1.7         | 0.0068             | 0.0002    | 4264.04                            | 0.50      | 1             | 1                                    |
| 14311_58_z8_L2  | 1,2,3  | 4.9        | 59                                      | -1.92  | 1.51        | -2.34  | 1.7         | 0.0059             | 0.0002    | 4255.58                            | 1.86      | 1             | 1                                    |
| 14311_58_z37_R  | 1,2,3  | 11.7       | 79                                      | -1.23  | 1.31        | -1.03  | 1.6         | 0.0055             | 0.0001    | 4334.24                            | 0.56      | 2             | 2                                    |
| 14311_58_z37_L2 | 1,2,3  | 3.9        | 55                                      | -0.14  | 1.53        | -0.73  | 1.7         | 0.0054             | 0.0002    | 4334.55                            | 3.74      | 2             | 2                                    |
| 14311_58_z40_R  | 1,2,3  | 12.6       | 80                                      | -4.14  | 1.38        | -4.46  | 1.7         | 0.0056             | 0.0002    | 4196.64                            | 0.88      | 1             | 1                                    |
| 14311_58_z40_L2 | 1,2,3  | 1.2        | 37                                      | -2.47  | 1.59        | -6.61  | 2.0         | 0.0051             | 0.0002    | 4220.57                            | 3.91      | 1             | 1                                    |
| 14311_58_z12_R  | 1,2,3  | 11.9       | 79                                      | -1.80  | 1.33        | -2.11  | 1.6         | 0.0066             | 0.0003    | 4289.21                            | 0.54      | 1             | 1                                    |
| 14311_58_z12_L2 | 1,2,3  | 4.2        | 56                                      | -1.73  | 1.46        | -2.84  | 1.8         | 0.0056             | 0.0002    | 4265.73                            | 0.71      | 1             | 1                                    |
| 14311_58_z59_R  | 1,2,3  | 164.6      | 190                                     | -5.85  | 1.29        | -5.86  | 1.6         | 0.0069             | 0.0003    | 3940.48                            | 0.50      | 1             | 1                                    |
| 14311_58_z59_L2 | 1,2,3  | 4.0        | 55                                      | -6.07  | 1.53        | -5.72  | 1.7         | 0.0072             | 0.0003    | 3939.08                            | 4.10      | 1             | 1                                    |
| 14311_58_z61_R  | 1,2,3  | 210.5      | 206                                     | -5.53  | 1.27        | -5.53  | 1.6         | 0.0070             | 0.0001    | 3948.29                            | 0.50      | 1             | 1                                    |
| 14311_58_z61_L2 | 1,2,3  | 5.5        | 61                                      | -6.12  | 1.47        | -6.30  | 1.7         | 0.0070             | 0.0002    | 3945.34                            | 1.53      | 1             | 1                                    |
| 14311_58_z34_R  | 1,2,3  | 20.0       | 94                                      | -3.30  | 1.34        | -3.59  | 1.6         | 0.0081             | 0.0002    | 4109.00                            | 0.57      | 1             | 1                                    |
| 14311_58_z34_L2 | 1,2,3  | 1.4        | 38                                      | -4.78  | 1.67        | -7.01  | 2.0         | 0.0076             | 0.0007    | 4109.28                            | 8.35      | 1             | 1                                    |
| 14163_65_z4_R   | 1,2,3  | 14.1       | 84                                      | -1.52  | 1.13        | -0.40  | 1.3         | 0.0074             | 0.0002    | 4250.67                            | 0.94      | 1             | 1                                    |
| 14163_65_z4_L2  | 1,2,3  | 2.0        | 44                                      | -2.64  | 1.47        | -2.34  | 1.1         | 0.0074             | 0.0004    | 4250.79                            | 1.07      | 1             | 1                                    |
| 72275A_z1_R     | 1,2,3  | 19.6       | 93                                      | -1.54  | 0.33        | -0.72  | 0.36        | 0.0070             | 0.0002    | 4336.84                            | 0.50      | 3             | 3                                    |
| 72275A_z1_L2    | 1,2,3  | 16.2       | 88                                      | -1.22  | 0.38        | -0.07  | 0.31        | 0.0061             | 0.0007    | 4336.22                            | 2.12      | 3             | 3                                    |
| 14311_58_z57_R  | 2,3    | 13.8       | 83                                      | -3.52  | 1.33        | -4.16  | 1.70        | 0.0141             | 0.0006    | 4314.69                            | 0.57      | 2             | 1                                    |
| 14311_58_z57_L2 |        | 19.6       | 93                                      | -0.38  | 1.37        | -0.93  | 1.70        | 0.0078             | 0.0004    | 4317.55                            | 0.55      | 2             | 1                                    |
| 14311_58_z15_R  | 2,3    | 57.3       | 133                                     | -4.88  | 1.24        | -5.38  | 1.60        | 0.0056             | 0.0003    | 4120.84                            | 0.52      | 1             | 1                                    |
| 14311_58_z15_L2 |        | 7.3        | 67                                      | 0.01   | 1.47        | 0.28   | 1.7         | 0.0033             | 0.0002    | 4293.17                            | 1.16      | 1             | 1                                    |
| 14311_58_z47_R  | 2,3    | 58.0       | 134                                     | -2.56  | 1.25        | -2.79  | 1.6         | 0.0093             | 0.0003    | 4225.71                            | 0.49      | 1             | 1                                    |
| 14311_58_z47_L2 |        | 10.9       | 77                                      | -0.54  | 1.27        | -1.59  | 1.7         | 0.0049             | 0.0001    | 4207.26                            | 0.61      | 1             | 1                                    |
| 14311_58_z6_R   | 2,3    | 5.0        | 59                                      | -4.09  | 1.45        | -4.12  | 1.7         | 0.0379             | 0.0006    | 4287.09                            | 0.77      | 1             | 1                                    |
| 14311_58_z6_L2  |        | 2.2        | 45                                      | 4.14   | 1.57        | 2.93   | 2.0         | 0.0179             | 0.0008    | 4287.33                            | 0.85      | 1             | 1                                    |
| 14311_58_z27_R  | 2,3    | 26.7       | 104                                     | -1.89  | 1.34        | -2.19  | 1.6         | 0.0147             | 0.0007    | 4305.90                            | 0.49      | 2             | 1                                    |
| 14311_58_z27_L2 |        | 5.4        | 61                                      | -0.33  | 1.52        | 1.36   | 1.8         | 0.0085             | 0.0004    | 4304.50                            | 0.57      | 2             | 1                                    |
| 14311_58_z18_R  | 2,3    | 25.3       | 102                                     | -3.06  | 1.40        | -3.93  | 1.7         | 0.0225             | 0.0007    | 4286.02                            | 0.50      | 1             | 1                                    |
| 14311_58_z18_L2 |        | 6.8        | 65                                      | 0.25   | 1.40        | -0.73  | 1.8         | 0.0142             | 0.0005    | 4270.90                            | 1.68      | 1             | 1                                    |
| 14163_65_z7_R   | 2,3    | 4.1        | 56                                      | 0.15   | 1.18        | -1.64  | 1.3         | 0.0144             | 0.0005    | 4336.46                            | 0.59      | 2             | 2                                    |
| 14163_65_z7_L2  |        | 8.5        | 71                                      | -3.39  | 1.16        | -2.5   | 1.1         | 0.0196             | 0.0004    | 4336.58                            | 1.70      | 2             | 2                                    |
| 14163_949_z3_R  | 2,3    | 20.8       | 95                                      | -1.66  | 1.03        | -2.34  | 1.0         | 0.0145             | 0.0003    | 4337.58                            | 0.51      | 1             | 1                                    |

|                 |     |       |     |       |      |       |      |        |        |         |       |   |   |
|-----------------|-----|-------|-----|-------|------|-------|------|--------|--------|---------|-------|---|---|
| 14163_949_z3_L2 |     | 5.9   | 63  | 0.69  | 1.15 | 0.87  | 1.0  | 0.008  | 0.0005 | 4334.88 | 2.30  | 1 | 1 |
| 15405_75_z1_R   | 2,3 | 14.9  | 85  | -1.09 | 0.99 | -1.15 | 1.0  | 0.0162 | 0.0006 | 4337.32 | 0.51  | 2 | 2 |
| 15405_75_z1_L2  |     | 4.6   | 57  | 1.97  | 0.80 | 2.31  | 1.0  | 0.0094 | 0.0004 | 4336.91 | 0.66  | 2 | 2 |
| 14311_58_z9_R   | 3   | 10.3  | 75  | -0.95 | 1.36 | -0.55 | 1.6  | 0.0088 | 0.0003 | 4335.49 | 0.75  | 2 | 2 |
| 14311_58_z7_R   | 3   | 6.1   | 63  | -1.78 | 1.49 | -2.57 | 1.8  | 0.0102 | 0.0004 | 4307.26 | 0.53  | 2 | 1 |
| 14311_58_z21_R  | 3   | 3.5   | 52  | -2.53 | 1.55 | -3.41 | 1.8  | 0.0206 | 0.0011 | 4334.94 | 0.54  | 2 | 2 |
| 14311_58_z38_R  | 3   | 12.6  | 81  | -1.53 | 1.31 | -2.15 | 1.6  | 0.01   | 0.0004 | 4295.71 | 0.53  | 1 | 1 |
| 14311_58_z43_L2 |     | 1.8   | 42  | -1.19 | 1.71 | -0.24 | 1.8  | 0.0093 | 0.0004 | 4322.34 | 4.02  | 2 | 1 |
| 14311_58_z69b_R | 3   | 29.2  | 107 | -3.59 | 1.36 | -3.89 | 1.6  | 0.0055 | 0.0003 | 4198.27 | 0.52  | 1 | 1 |
| 14311_58_z69a_R | 3   | 45.2  | 123 | -3.42 | 1.24 | -3.74 | 1.6  | 0.0055 | 0.0003 | 4206.03 | 0.53  | 1 | 1 |
| 14311_58_z71_R  | 3   | 67.0  | 141 | -1.64 | 1.23 | -2.13 | 1.6  | 0.0095 | 0.0003 | 4249.09 | 0.49  | 1 | 1 |
| 14311_58_z71_L2 |     | 4.6   | 58  | 1.4   | 1.51 | 0.59  | 1.8  | 0.0071 | 0.0006 | 4243.67 | 1.79  | 1 | 1 |
| 14311_58_z14_R  | 3   | 25.1  | 101 | -3.76 | 1.36 | -4.15 | 1.6  | 0.0094 | 0.0003 | 4096.95 | 0.51  | 1 | 1 |
| 14311_58_z64_R  | 3   | 146.4 | 183 | -6.16 | 1.27 | -5.89 | 1.5  | 0.007  | 0.0002 | 3940.42 | 0.49  | 1 | 1 |
| 14311_58_z58_R  | 3   | 56.8  | 133 | -1.22 | 1.30 | -1.77 | 1.6  | 0.0303 | 0.0005 | 4290.14 | 0.49  | 1 | 1 |
| 14311_58_z58_L2 |     | 7.9   | 69  | 8.57  | 1.48 | 8.71  | 1.8  | 0.0169 | 0.0005 | 4282.34 | 0.53  | 1 | 1 |
| 14311_58_z60_R  | 3   | 28.1  | 105 | -6.09 | 1.36 | -6.23 | 1.6  | 0.0075 | 0.0002 | 3942.92 | 0.54  | 1 | 1 |
| 14311_58_z60_L2 |     | 1.1   | 35  | 13.64 | 1.36 | 14.08 | 1.4  | 0.0075 | 0.0003 | 3944.21 | 8.83  | 1 | 1 |
| 14311_58_z24_R  | 3   | 39.8  | 118 | -1.72 | 1.33 | -2.21 | 1.7  | 0.0069 | 0.0006 | 4250.18 | 0.55  | 1 | 1 |
| 14311_58_z24_L2 |     | 3.5   | 52  | 3.63  | 1.26 | 2.87  | 1.6  | 0.0059 | 0.0002 | 4241.43 | 1.70  | 1 | 1 |
| 14163_65_z3_L2  |     | 3.7   | 53  | -1.08 | 0.94 | -1.1  | 1.1  | 0.0121 | 0.0006 | 4336.53 | 2.51  | 2 | 2 |
| 14163A_z9_L1    |     | 9.5   | 73  | -1.50 | 0.40 | -1.24 | 0.29 | 0.0138 | 0.0005 | 4268.33 | 2.44  | 3 | 3 |
| 14163A_z26_L1   |     | 9.0   | 72  | 0.07  | 0.47 | 0.89  | 0.58 | 0.0046 | 0.0002 | 4337.07 | 30.35 | 3 | 3 |
| 14163A_z26_L2   |     | 10.1  | 75  | -2.64 | 0.37 | -1.76 | 0.44 | 0.0044 | 0.0001 | 4255.67 | 16.19 | 3 | 3 |
| 14163A_z89_R    | 3   | 9.2   | 73  | -2.34 | 0.33 | -1.42 | 0.37 | 0.0058 | 0.0002 | 4295.85 | 0.83  | 3 | 3 |
| 14321A_z3_L1    |     | 71.4  | 144 | -2.17 | 0.22 | -1.87 | 0.33 | 0.0105 | 0.0017 | 4220.48 | 0.60  | 3 | 3 |
| 14321A_z3_L2    |     | 40.3  | 119 | -3.80 | 0.41 | -3.35 | 0.28 | 0.0146 | 0.0006 | 4217.48 | 0.55  | 3 | 3 |
| 72275A_z1_L1    |     | 22.3  | 98  | -0.60 | 0.35 | -0.55 | 0.29 | 0.0064 | 0.0003 | 4331.63 | 3.32  | 3 | 3 |

\*Errors include uncertainties from both CHUR and zircon measurements. See the Excel spreadsheet in Datasets S1 for details on the data reduction.

<sup>a</sup> <sup>207</sup>Pb/<sup>206</sup>Pb ages corrected for initial Th/U disequilibrium using radiogenic <sup>208</sup>Pb and Th/U[magma] = 3.50000.

References: 1. This study; 2. Barboni *et al.* (3); 3. Chen *et al.* (2)

## SI References

1. D. J. Taylor, K. D. McKeegan, T. M. Harrison, Lu–Hf zircon evidence for rapid lunar differentiation. *Earth and Planetary Science Letters* **279**, 157-164 (2009).
2. X. Chen *et al.*, Methodologies for  $^{176}\text{Lu}$ – $^{176}\text{Hf}$  analysis of zircon grains from the Moon and beyond. *ACS Earth and Space Chemistry* 10.1021/acsearthspacechem.3c00093 (2023).
3. M. Barboni *et al.*, High precision U–Pb zircon dating pinpoints a major magmatic event on the Moon at 4.337 Ga. *Science Advances* **10**, eadn9871 (2024).
4. C. Meyer, I. S. Williams, W. Compston, Uranium-lead ages for lunar zircons: Evidence for a prolonged period of granophyre formation from 4.32 to 3.88 Ga. *Meteoritics & Planetary Science* **31**, 370-387 (1996).
5. C. Meyer, Lunar sample compendium. (2005).
6. L. A. Haskin, R. L. Korotev, J. J. Gillis, B. L. Jolliff (2002) Stratigraphies of Apollo and Luna highland landing sites and provenances of materials from the perspective of basin impact ejecta modeling. in *Lunar and Planetary Science Conference*, p 1364.
7. R. Morrison, V. Oberbeck (1975) Geomorphology of crater and basin deposits–Emplacement of the Fra Mauro formation. in *Lunar Science Conference, 6th, Houston, Tex., March 17-21, 1975, Proceedings. Volume 3.(A78-46741 21-91)* New York, Pergamon Press, Inc., 1975, p. 2503-2530.
8. F. J. Stadermann, E. Heusser, E. K. Jessberger, S. Lingner, D. Stöffler, The case for a younger Imbrium basin: New  $^{40}\text{Ar}$ – $^{39}\text{Ar}$  ages of Apollo 14 rocks. *Geochimica et Cosmochimica Acta* **55**, 2339-2349 (1991).
9. R. Drozd, C. Hohenberg, C. Morgan, C. Ralston, Cosmic-ray exposure history at the Apollo 16 and other lunar sites: lunar surface dynamics. *Geochimica et Cosmochimica Acta* **38**, 1625-1642 (1974).
10. R. E. Merle *et al.*, Origin and transportation history of lunar breccia 14311. *Meteoritics & Planetary Science* **52**, 842-858 (2017).
11. M. Hopkins, S. J. Mojzsis, A protracted timeline for lunar bombardment from mineral chemistry, Ti thermometry and U–Pb geochronology of Apollo 14 melt breccia zircons. *Contributions to Mineralogy and Petrology* **169**, 1-18 (2015).
12. J. M. Devine, D. S. McKay, J. J. Papike, Lunar regolith: Petrology of the <10  $\mu\text{m}$  fraction. *Journal of Geophysical Research: Solid Earth* **87**, A260-A268 (1982).
13. T. Labotka, M. Kempa, C. White, J. Papike, J. Laul (1980) The lunar regolith–Comparative petrology of the Apollo sites. In: *Lunar and Planetary Science Conference, 11th, Houston, TX, March 17-21, 1980, Proceedings. Volume 2.(A82-22296 09-91)* New York, Pergamon Press, 1980, p. 1285-1305.
14. C. A. Crow, K. D. McKeegan, D. E. Moser, Coordinated U–Pb geochronology, trace element, Ti-in-zircon thermometry and microstructural analysis of Apollo zircons. *Geochimica et Cosmochimica Acta* **202**, 264-284 (2017).
15. M. Grange, A. Nemchin, R. Pidgeon, The effect of 1.9 and 1.4 Ga impact events on 4.3 Ga zircon and phosphate from an Apollo 15 melt breccia. *Journal of Geophysical Research: Planets* **118**, 2180-2197 (2013).
16. P. H. Warren, G. J. Taylor, K. Keil, D. N. Shirley, J. T. Wasson, Petrology and chemistry of two “large” granite clasts from the Moon. *Earth and Planetary Science Letters* **64**, 175-185 (1983).

17. A. Nemchin, R. Pidgeon, M. Whitehouse, J. P. Vaughan, C. Meyer, SIMS U–Pb study of zircon from Apollo 14 and 17 breccias: implications for the evolution of lunar KREEP. *Geochimica et Cosmochimica Acta* **72**, 668-689 (2008).
18. A. Nemchin, M. Whitehouse, R. Pidgeon, C. Meyer, Oxygen isotopic signature of 4.4–3.9 Ga zircons as a monitor of differentiation processes on the Moon. *Geochimica et Cosmochimica Acta* **70**, 1864-1872 (2006).
19. M. Grange, R. Pidgeon, A. Nemchin, N. E. Timms, C. Meyer, Interpreting U–Pb data from primary and secondary features in lunar zircon. *Geochimica et Cosmochimica Acta* **101**, 112-132 (2013).
20. A. Nemchin *et al.*, Timing of crystallization of the lunar magma ocean constrained by the oldest zircon. *Nature geoscience* **2**, 133-136 (2009).
21. J. M. Mattinson, Zircon U–Pb chemical abrasion (“CA-TIMS”) method: combined annealing and multi-step partial dissolution analysis for improved precision and accuracy of zircon ages. *Chemical Geology* **220**, 47-66 (2005).
22. M. Barboni *et al.*, Early formation of the Moon 4.51 billion years ago. *Science advances* **3**, e1602365 (2017).
23. A. Pourmand, N. Dauphas, Distribution coefficients of 60 elements on TODGA resin: application to Ca, Lu, Hf, U and Th isotope geochemistry. *Talanta* **81**, 741-753 (2010).
24. J. Zhang, N. Dauphas, A. M. Davis, A. Pourmand, A new method for MC-ICPMS measurement of titanium isotopic composition: Identification of correlated isotope anomalies in meteorites. *Journal of Analytical Atomic Spectrometry* **26**, 2197-2205 (2011).
25. C. Münker, S. Weyer, E. Scherer, K. Mezger, Separation of high field strength elements (Nb, Ta, Zr, Hf) and Lu from rock samples for MC-ICPMS measurements. *Geochemistry, Geophysics, Geosystems* **2** (2001).
26. T. Iizuka, T. Yamaguchi, Y. Hibiya, Y. Amelin, Meteorite zircon constraints on the bulk Lu–Hf isotope composition and early differentiation of the Earth. *Proceedings of the National Academy of Sciences* **112**, 5331-5336 (2015).
27. H. Gerstenberger, G. Haase, A highly effective emitter substance for mass spectrometric Pb isotope ratio determinations. *Chemical geology* **136**, 309-312 (1997).
28. D. Szymanowski, B. Schoene, U–Pb ID-TIMS geochronology using ATONA amplifiers. *Journal of Analytical Atomic Spectrometry* **35**, 1207-1216 (2020).
29. U. Söderlund, P. J. Patchett, J. D. Vervoort, C. E. Isachsen, The  $^{176}\text{Lu}$  decay constant determined by Lu–Hf and U–Pb isotope systematics of Precambrian mafic intrusions. *Earth and Planetary Science Letters* **219**, 311-324 (2004).
30. T. Hayakawa, T. Shizuma, T. Iizuka, Half-life of the nuclear cosmochronometer  $^{176}\text{Lu}$  measured with a windowless  $4\pi$  solid angle scintillation detector. *Communications Physics* **6**, 299 (2023).
31. J. N. Connelly *et al.*, The absolute chronology and thermal processing of solids in the solar protoplanetary disk. *Science* **338**, 651-655 (2012).
32. A. Bouvier, J. D. Vervoort, P. J. Patchett, The Lu–Hf and Sm–Nd isotopic composition of CHUR: constraints from unequilibrated chondrites and implications for the bulk composition of terrestrial planets. *Earth and Planetary Science Letters* **273**, 48-57 (2008).

33. P. Sprung, T. Kleine, E. E. Scherer, Isotopic evidence for chondritic Lu/Hf and Sm/Nd of the Moon. *Earth and Planetary Science Letters* **380**, 77-87 (2013).
34. A. M. Gaffney, L. E. Borg, A young solidification age for the lunar magma ocean. *Geochimica et Cosmochimica Acta* **140**, 227-240 (2014).
35. T. Harrison *et al.*, Heterogeneous Hadean hafnium: evidence of continental crust at 4.4 to 4.5 Ga. *Science* **310**, 1947-1950 (2005).
36. M. Barboni *et al.*, High precision U-Pb zircon dating identifies a major magmatic event on the Moon at 4.338 Ga. *Science Advances* **10**, eadn9871 (2024).
37. L. E. Borg *et al.*, Isotopic evidence for a young lunar magma ocean. *Earth and Planetary Science Letters* **523**, 115706 (2019).
38. L. E. Borg, R. W. Carlson, The evolving chronology of Moon formation. *Annual Review of Earth and Planetary Sciences* **51**, 25-52 (2023).
39. N. Marks, L. Borg, I. Hutcheon, B. Jacobsen, R. Clayton, Samarium-neodymium chronology of an Allende calcium-aluminum-rich inclusion with implications for  $^{146}\text{Sm}$  isotopic evolution. *Earth Planet. Sci. Lett* **405**, 15-24 (2014).
40. L. E. Borg, A. M. Gaffney, C. K. Shearer, A review of lunar chronology revealing a preponderance of 4.34–4.37 Ga ages. *Meteoritics & Planetary Science* **50**, 715-732 (2015).
41. Y. Amelin, E. Rotenberg, Sm–Nd systematics of chondrites. *Earth and Planetary Science Letters* **223**, 267-282 (2004).
42. L. Fang *et al.*, Half-life and initial Solar System abundance of  $^{146}\text{Sm}$  determined from the oldest andesitic meteorite. *Proceedings of the National Academy of Sciences* **119**, e2120933119 (2022).
43. C. Burkhardt *et al.*, A nucleosynthetic origin for the Earth's anomalous  $^{142}\text{Nd}$  composition. *Nature* **537**, 394-398 (2016).
44. L. Nyquist *et al.*,  $^{146}\text{Sm}$ - $^{142}\text{Nd}$  formation interval for the lunar mantle. *Geochimica et Cosmochimica Acta* **59**, 2817-2837 (1995).
45. M. Boyet, R. W. Carlson, A highly depleted moon or a non-magma ocean origin for the lunar crust? *Earth and Planetary Science Letters* **262**, 505-516 (2007).
46. A. D. Brandon *et al.*, Re-evaluating  $^{142}\text{Nd}/^{144}\text{Nd}$  in lunar mare basalts with implications for the early evolution and bulk Sm/Nd of the Moon. *Geochimica et Cosmochimica Acta* **73**, 6421-6445 (2009).
47. J. E. Dickinson Jr, P. Hess, Zircon saturation in lunar basalts and granites. *Earth and Planetary Science Letters* **57**, 336-344 (1982).
48. P. H. Warren, J. T. Wasson, The origin of KREEP. *Reviews of Geophysics* **17**, 73-88 (1979).
49. G. A. Gualda, M. S. Ghiorso, R. V. Lemons, T. L. Carley, Rhyolite-MELTS: a modified calibration of MELTS optimized for silica-rich, fluid-bearing magmatic systems. *Journal of Petrology* **53**, 875-890 (2012).
50. L. J. Crisp, A. J. Berry, A new model for zircon saturation in silicate melts. *Contributions to Mineralogy and Petrology* **177**, 71 (2022).